ISSN 0020-4412, Instruments and Experimental Techniques, 2013, Vol. 56, No. 2, pp. 185–192. © Pleiades Publishing, Ltd., 2013.
Original Russian Text © Yu.I. Isakova, A.I. Pushkarev, 2013, published in Pribory i Tekhnika Eksperimenta, 2013, No. 1, pp. 69–76.

GENERAL EXPERIMENTAL TECHNIQUES

Thermal Imaging Diagnostics of Powerful Ion Beams

Yu. I. Isakova and A. I. Pushkarev

Tomsk Polytechnic University, pr. Lenina 30, Tomsk, 634050 Russia

e-mail: aipush@mail.ru

Received April 16, 2012

Abstract—Thermal imaging diagnostics of the total energy of a pulsed ion beam and energy-density distribution over the cross section is described. The diagnostics was tested on the ТЕМП-4М accelerator in the conditions of formation of two pulses: (i) the first plasma-forming pulse is negative (300–500 ns, 100–150 kV) and (ii) the second generated one is positive (150 ns, 250–300 kV). The beam composition includes carbon ions (85%) and protons, and the power density is 0.2–3.0 J/cm^2 (for various diodes). The diagnostics was applied in studies of the powerful ion beam, formed by an ion diode with self insulation (two-pulse mode) and external magnetic insulation in the single-pulse mode. The diagnostics was intended to measure the beam energy density in a range of 0.05–5.00 J/cm^2 in the absence of erosion and ablation processes on the target. When an infrared camera with a 140 × 160-pixel matrix is used, the spatial resolution is 0.9 mm. The measurement time does not exceed 0.1 s.

DOI: 10.1134/S0020441213020085

INTRODUCTION

The action of charged particle beams on metals and alloys initiates thermal, thermo-mechanical, and diffusion processes in them, leading to their structural and phase transformations [1]. As a result, the properties of materials, such as hardness, strength, and wear-resistance, change, thus the operating characteristics of the products improve. The concentration of ions in a beam of gigawatt power does not exceed 10^{12} cm^{-3}, and the main factor that determines changes in the product properties is not the ion implantation but a thermal effect. Therefore, to control and optimize conditions for processing products with a powerful ion beam (PIB), it is necessary to record, first of all, the ion-beam energy density and cross-sectional beam uniformity.

The calorimetric methods are widespread for measuring the cross-sectional energy distributions of charged particle beams. In 1976, this method was for the first time applied to measure the PIB parameters [2]. The cross-sectional beam energy distribution is usually measured by the sectionalized calorimeter [3]. However, a complex design of the calorimeter is required to ensure a spatial resolution of 1–2 mm with a PIB area of >20 cm^2 and the measurement process takes a good deal of time. Therefore, this method does not allow one to promptly control operation conditions of the PIB generator during product processing.

In 1997, it was proposed in [4] to use an infrared camera for measuring the energy density distribution of a pulsed ion beam. They studied the PIB with an energy density of >5 J/cm^2, formed by a diode with external magnetic insulation in the single-pulse mode. Basic attention was paid to accounting for the influence of the ablation process of the target material on the results of thermal-imaging measurements.

To use correctly the thermal-imaging diagnostics in the process of controlling the PIB with a low energy density, it is necessary to estimate the contribution of electrons, generated during the first pulse and afterpulses, explosion-emission plasma, etc., to the target heating. The purpose of this work is to design the thermal-imaging diagnostics for measuring the energy-density distribution over the cross section of gigawatt-power pulsed ion beams.

MEASUREMENT PROCEDURE OF THE PIB ENERGY DENSITY DISTRIBUTION

The studies were performed on the ТЕМП-4М accelerator [5, 6] configured in the double pulse mode: (i) the first pulse is negative (300–500 ns, 100–150 kV) and (ii) the second pulse is positive (150 ns, 250–300 kV). The beam consists of carbon ions (85%) and protons, the energy density on the target is 0.2–3.0 J/cm^2 (for various diodes), and the pulse repetition rate is 5–10 pulses/min. The diode with self-magnetic insulation with an explosion-emission cathode, operating in the double-pulse mode, is used to generate the PIB. The recording scheme and waveforms that reflect operation of the ТЕМП-4М accelerator in the double-pulse mode are shown in Fig. 1.

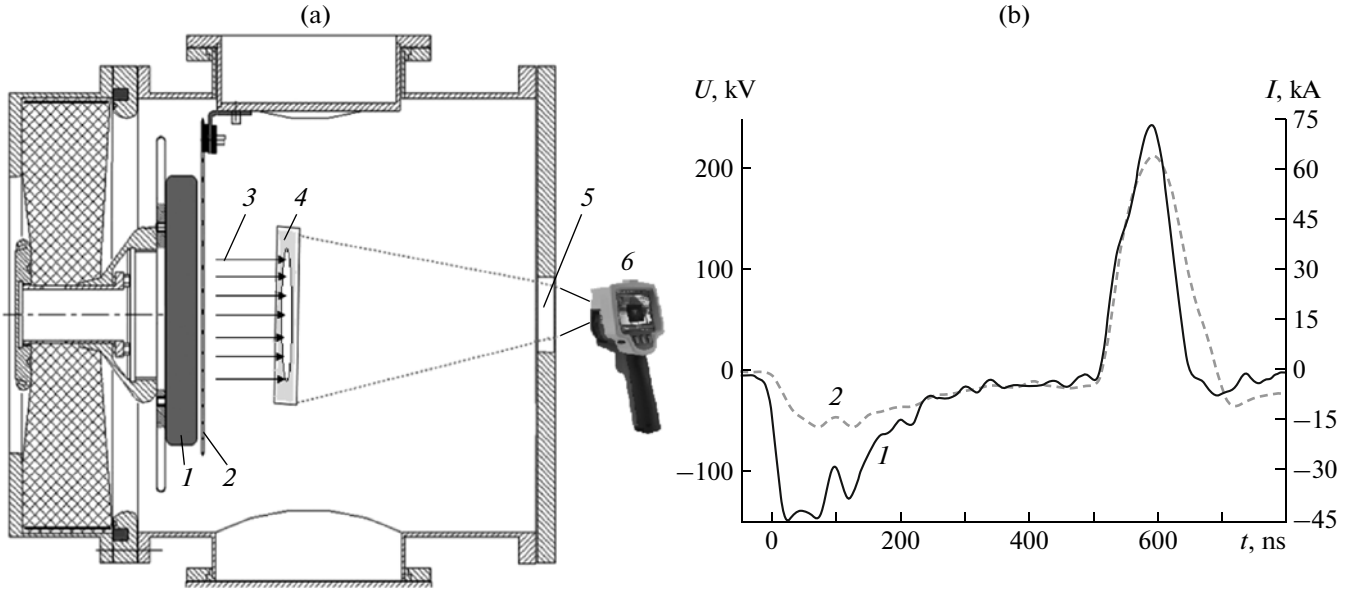

Fig. 1. (a) Diode assembly scheme: (*1*) potential electrode, (*2*) grounded electrode, (*3*) ion beam, (*4*) target, (*5*) CaF_2 window, and (*6*) thermal imager; (b) waveforms of the accelerating voltage (*1*) and total current (*2*) in the flat strip diode.

The main part of the studies was performed using a 22.0 × 4.5-cm size flat strip diode with an A-K gap spacing of 7–9 mm. The potential electrode is made of graphite, the grounded electrode is made of stainless steel with 0.4 × 5.0-cm size slits, and the transparency is 60%. The total diode current was measured with a Rogowski coil. The ion current density, composition, and energy spectrum of the PIB were determined by the time-of-flight procedure [7] using a collimated Faraday cup (CFC) with magnetic insulation of electrons ($B = 0.4$ T).

The voltage at the potential electrode was controlled with a high-frequency high-voltage divider, placed ahead of the diode assembly, and with a differential voltage divider [8]. The electric signals from sensors were recorded with a 2024B Tektronix oscilloscope (200 MHz, 5×10^9 samples/s). The design of the diode and location and calibration of the diagnostic equipment of the ТЕМП-4М accelerator can be found elsewhere [9, 10].

The PIB parameters were also diagnosed from the thermal print on the target using the Fluke TiR10 infrared camera (the spectral range is 7–14 μm). A brass plate with a thickness of 100 or 220 μm was used as a target, since it has a low heat capacity and low thermal conductivity, being important for thermal-imaging diagnostics. To increase the brass emissivity, the back (from the ion beam) side of the target was sprayed with black dull paint ($\varepsilon = 0.90$). The lifetime of this target exceeds 10^4 PIB pulses.

The thermal print of the beam was recorded through the exit window, located on the flange of the diode chamber (see Fig. 1). A calcium fluoride (CaF_2) parallel-sided plate was used as a window. The transmission spectrum of the optical window was measured with a Nicolet 5700 infrared Fourier spectrometer. Calcium fluoride features incomplete transmission in a spectral range of 7–14 μm; therefore, readouts of the infrared camera that records the heat flow transmitted through the CaF_2 window differ from actual temperature values of the target.

The diagnostic equipment was calibrated before the studies. Hot water was poured into a brass bath, the outer side of which was sprayed with black dull paint. The bath was placed into the diode chamber on the target spot. The water temperature was measured with the infrared camera (through the CaF_2 window) and the thermocouple was placed in the bath. The readouts of the thermocouple were also compared to those of the mercurial thermometer.

Five identical measurements were performed to correctly determine the transmission spectrum of the window. The calibration curve was approximated by a linear function, and the coefficients were calculated by the least-squares method in the Origin 7.5 program. The approximation error did not exceed 5%. The obtained linear function was further used to calculate the PIB energy density.

When the viewing angle is 25° and the minimum focal length is 30 cm for the Fluke TiR10 infrared camera, the size of the scanned object is 12.7 cm. For the 140 × 160 -pixel matrix of the Fluke TiR10 thermal imager, the spatial resolution is 0.8–0.9 mm.

The amount of energy Q, J, released in the target under exposure is equal to

$$Q = c_v m \Delta T = c_v S d \rho \Delta T,$$

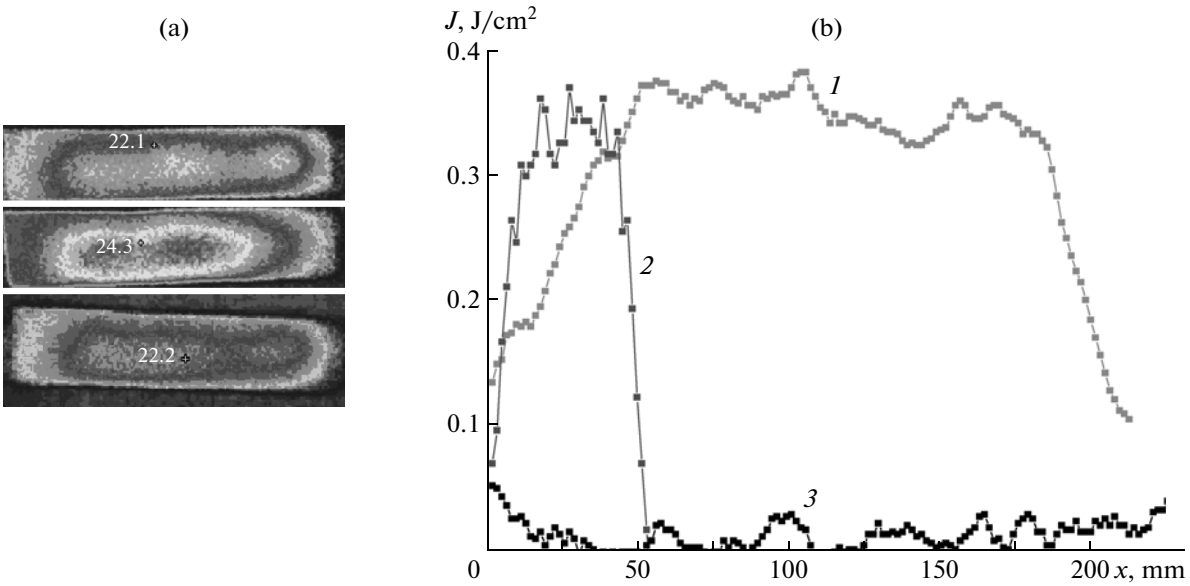

Fig. 2. (a) Thermograms of the PIB and (b) energy-density distribution on the target in the (*1*) longitudinal and (*2*) transverse sections. Curve *3* is the initial thermal background of the target.

where c_v is the specific heat capacity, S is the area of the target, d is the thickness of the target, ρ is the density, and ΔT is the target heating.

Then, the PIB energy density $J(x, y)$, J/cm^2, can be determined from the formula

$$J(x,y) = \frac{Q}{S} = c_v d\rho\Delta T(x,y).$$

The thermograms, recorded by the infrared camera, were processed using the SmartView™ program. When the minimum rated temperature sensitivity of the Fluke TiR10 infrared camera is 0.2°C, the minimum energy density for a 0.2-mm-thick brass target (with consideration for the heat flow attenuation in the exit window) is 0.02 J/cm^2. A thinner foil or a material with a smaller heat capacity can be used to increase the sensitivity of the thermal-imaging diagnostics.

After target heating by the powerful ion beam, the temperature of the other surface was viewed with the infrared camera (see Fig. 1). The time $\tau_{0.5}$, s, required for raising the temperature of the rear (with respect to the PIB) surface of the target by 50% from the maximum can be calculated from the ratio [11]

$$\tau_{0.5} = \frac{0.14d^2}{a},$$

where d, m, is the thickness of the target and a, m^2/s, is the thermal diffusivity.

For a 220-μm-thick brass target (the thermal diffusivity of brass is 3×10^{-5} m^2/s), the warming-up time over the entire thickness does not exceed 0.25 ms.

When the ТЕМП-4М accelerator operates, the bremsstrahlung X-ray radiation is formed the absorbed dose rate of which exceeds the permissible standards for the maintenance personnel. Therefore, there is a delay of 2–3 s between the shot and measurement of the thermal field on the target.

The same PIB thermal print on the target was measured at various time intervals to estimate the procedure error due to distortions of the thermal-field profile on cooling. The performed studies of the cooling dynamics of the 220-μm-thick brass target after the PIB action (with an energy density of ≈2 J/cm^2) showed that within 5 s, the half-height temperature distribution width increases by 16%. The maximum delay between the PIB pulse generation and measurement of the thermal print on the target does not exceed 3 s; therefore, the thermal-imaging procedure error due to distortions of the thermal-field profile on cooling of the brass target does not exceed 10%. When the PIB with an energy density of <1 J/cm^2 is recorded, the error is even lower.

In spite of the temperature reduction at the maximum heating point, the total thermal print energy, which was determined from the average temperature calculated by the SmartView™ program for the entire brass target, remained unchanged and was equal to 95 ± 5 J. This indicates the fact that the temperature reduction at the maximum heating point is caused by the thermal diffusivity of the target material but not by thermal radiation.

The target cooling rate after the PIB action depends on its heating temperature, determined by the ion-beam energy density. The 100-μm-thick stainless steel target was used to decrease the thermal-imaging procedure error in studies of the PIB with an energy density of >2 J/cm^2. The thermal diffusivity of stainless steel is twofold lower than that of brass; therefore,

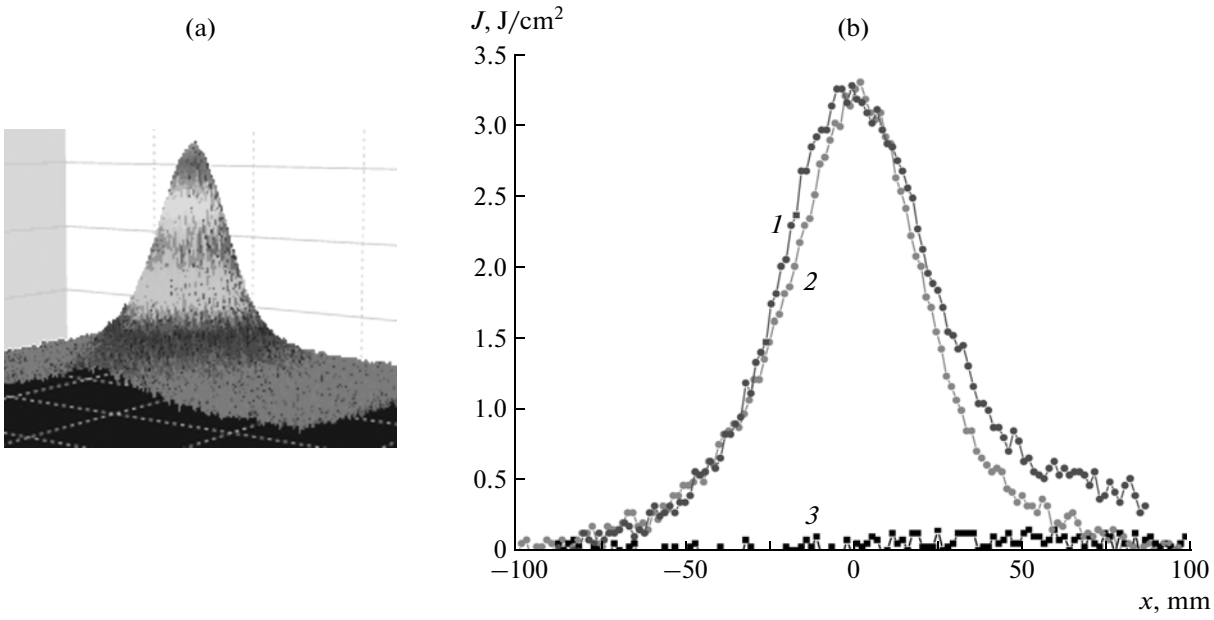

Fig. 3. (a) The PIB thermogram in the focal plane of the focusing strip diode and (b) the energy-density distribution in the (*1*) horizontal and (*2*) vertical sections. Curve *3* is the initial thermal background of the target.

the thermal-imaging procedure error due to distortions of the thermal-field profile on cooling of the stainless steel target does not exceed 5%.

THE PIB ENERGY DENSITY DISTRIBUTION OVER THE CROSS SECTION

The designed thermal-imaging diagnostics was used to control the uniformity of the PIB, formed by the diode with self-magnetic insulation. When the anode–cathode gap spacing is increased at the end of the flat strip diode (as compared to the beginning), a more uniform distribution of the PIB energy density is achieved. Figure 2 shows the measurement results of the energy-density distribution over the PIB cross section in the flat strip diode, when the anode–cathode gap is 8 mm at the beginning of the diode and 10 mm at the end. The thermograms of three different PIB pulses are shown. The 100-μm-thick brass target was used, and the distance from the diode to the target was 12 cm.

A typical PIB thermal print of the focusing strip diode is shown in Fig. 3. The 100-μm-thick stainless steel target was used, and the diode–target distance was 14 cm. The analysis of the PIB thermograms of the focusing diode showed that the nonuniformity of the ion beam density along the length of the focusing diode weakly influences the energy-density distribution at the focus. The width of the half-height thermal print (in the horizontal direction) is close to the width of the strip diode (45 mm), indicating a small PIB divergence.

ANALYSIS OF THE CONTRIBUTION OF ELECTRONS TO THE TARGET HEATING

In the ion diode operating in the double-pulse mode, the thermal print on the target can be formed by electrons that reached the target during the first pulse and by ions during the second pulse. The thermal-imaging diagnostics does not allow one to differentiate their contributions to the target heating. During the first pulse, electrons start from the potential electrode and travel in the anode–cathode gap to the grounded electrode, which is connected to the housing of the diode chamber only at one side (see Fig. 1). Later, electrons travel along the electrode to the grounding point, forming a magnetic field in the gap, whose magnetic-induction vector is perpendicular to the electric-intensity vector. Therefore, as the electrons cross the anode–cathode gap, the subsequent electrons fall within the magnetic field and drift to the free end of the diode [9]. Reaching the end of the drift region, the electrons can reliese to the target, causing its heating.

To measure the energy density of electrons that were accelerated in the anode–cathode gap of the strip diode and reached the target, the Faraday cup without magnetic insulation of electrons was used. It is made out of the conventional BNC connector, the diameter of the collector is 8 mm, and the diameter of the aperture in the cover is 4 mm. The measuring scheme for the electron beam current, which is formed by the diode during the first pulse and the Faraday cup design, are shown in Fig. 4. Typical waveforms of the accelerating voltage and current recorded by the Faraday cup at a distance of 12 cm from the flat strip diode are shown in Fig. 5.

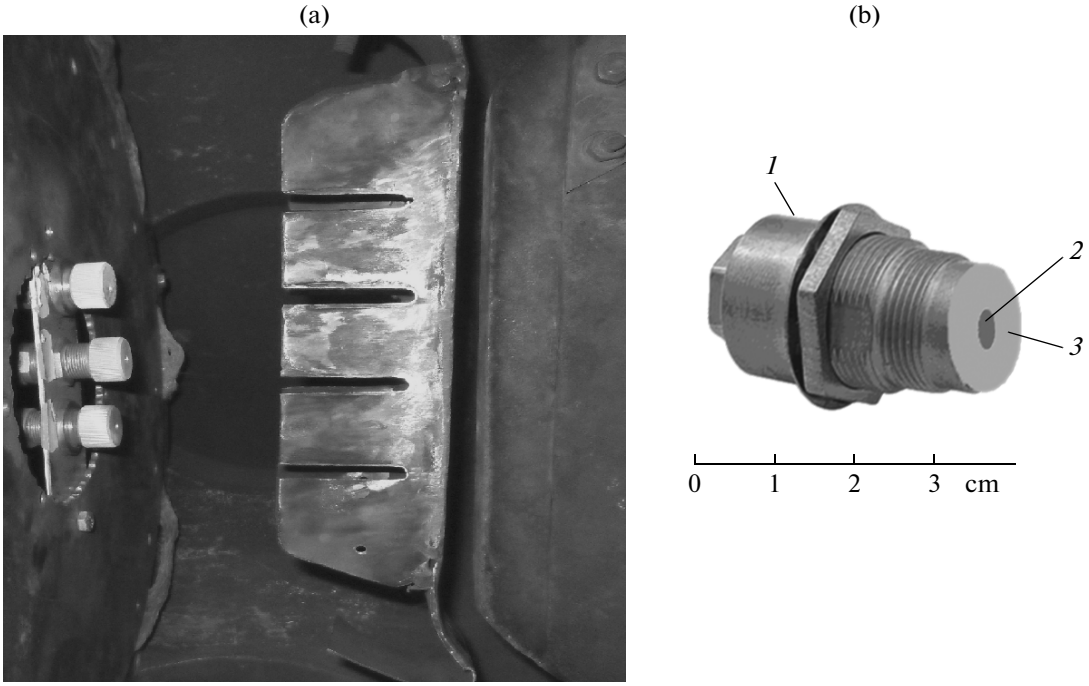

Fig. 4. (a) The measurement scheme and (b) the Faraday cup design: (*1*) BNC connector, (*2*) 4-mm-diameter hole, and (*3*) screen.

The performed studies showed that, in the used Faraday cup design, the noise level does not exceed ±1 A/cm^2, thus corresponding to an energy density of 6.0 ± 1.6 mJ/cm^2. The Faraday cup collectors were covered with a 40-μm-thick aluminum foil to determine the energy spectrum of electrons generated during the first voltage pulse. The measurement results are shown in Fig. 6. According to the obtained results, the energy of electrons that reach the target during the first pulse exceeds 50 keV, corresponding to an electron-energy density (the integral of the product of the voltage by the Faraday cup electron current density during the first pulse) of 64 ± 16 mJ/cm^2. This is significantly smaller than the PIB energy density measured by the thermal-imaging method. Similar measurements were also performed for the focusing strip diode. The average electron-energy density at the focus of the ion diode (the integral of the product of the voltage by the electron current density from the Faraday cup during the first pulse) was 10–15 mJ/cm^2, being significantly smaller than the PIB energy density at the focus of the strip focusing diode, measured by the thermal-imaging method (see Fig. 3).

CONTRIBUTION OF THE EXPLOSION-EMISSION PLASMA TO THE TARGET HEATING

In the diode with an explosion-emission cathode, plasma may contribute to the target heating due to expansion from the electrode surface. It is difficult to directly measure its influence; therefore, evaluation data are presented in this section. Based on the literature review and hydrodynamic simulation of the explosion-emission plasma spread, Proskurovskii showed in [12] that the specific energy contribution of the nanosecond pulse generator to the explosion-emission plasma formation is $\approx 2 \times 10^4$ J/g of the cathode material. Paper [12] gives experimental values of the material removal from the peak of a single molybdenum edge due to the explosive emission, namely, within one current pulse with an 80-ns duration, the ablation of a 20-μm-diameter edge is $(2–8) \times 10^{-9}$ g.

The number of emitting centers is equal to the ratio of the cathode area to the area of one hexahedron that forms the honeycomb structure of emission centers [13]:

$$N = \frac{1.15S}{b^2},$$

where S is the area of the potential electrode, and b is the distance between adjacent emission centers.

The minimum distance between discrete emission centers is determined by the screening effect of the electric field around the center [14] and equal to two screening radii r, cm:

$$r = 500 d_0 I_1^{1/2} U^{-3/4},$$

where d_0 is the anode–cathode gap spacing, I_1 is the current of a single emission center, and U is the accelerating voltage.

The screening radius is equal to 5–6 mm for an electron current from one emission center of 90 A [14] and

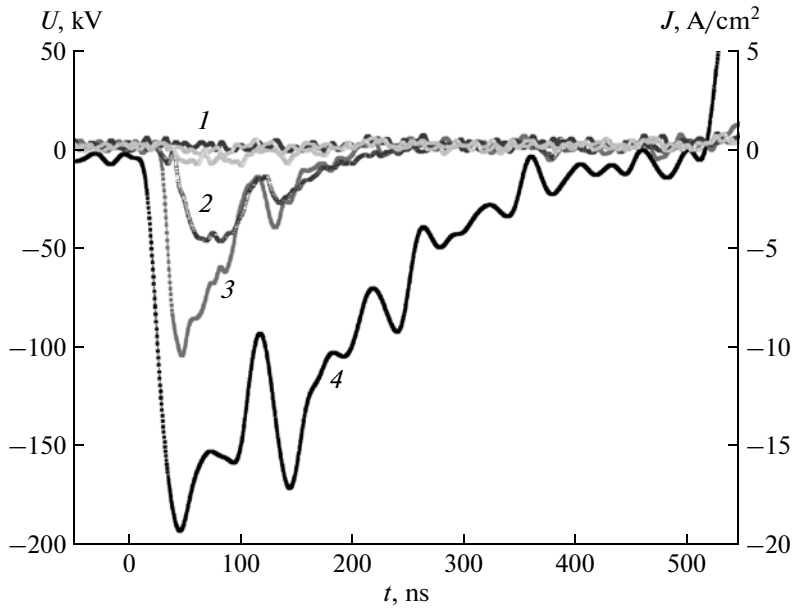

Fig. 5. Oscillograms of the current density, recorded by (*1*) three closed Faraday cups and (*2*, *3*) two open Faraday cups, and (*4*) of the accelerating voltage.

an average voltage of 100–120 kV during the emission center formation (see Fig. 1). In this case, 80–100 explosion-emission centers are formed on the electrode with an area of 80–100 cm^2. The power consumption on their formation does not exceed 16 mJ.

In addition, the performed experimental studies of the energy balance of the planar diode with a graphite explosion-emission cathode during the electron-beam generation showed [15] that the energy losses in the diode are in proportion to the anode–cathode gap spacing. The general behavior of the dependence for cathodes made of various materials indicates the fact that the power consumption of the diode is related not to the explosion-emission formation process but to the transportation process of beam electrons in the anode–cathode gap. The power consumption on the explosion-emission plasma formation does not exceed 1 J with an anode area of 16–20 cm^2. Therefore, in the ion diode with a passive anode in double-pulse mode,

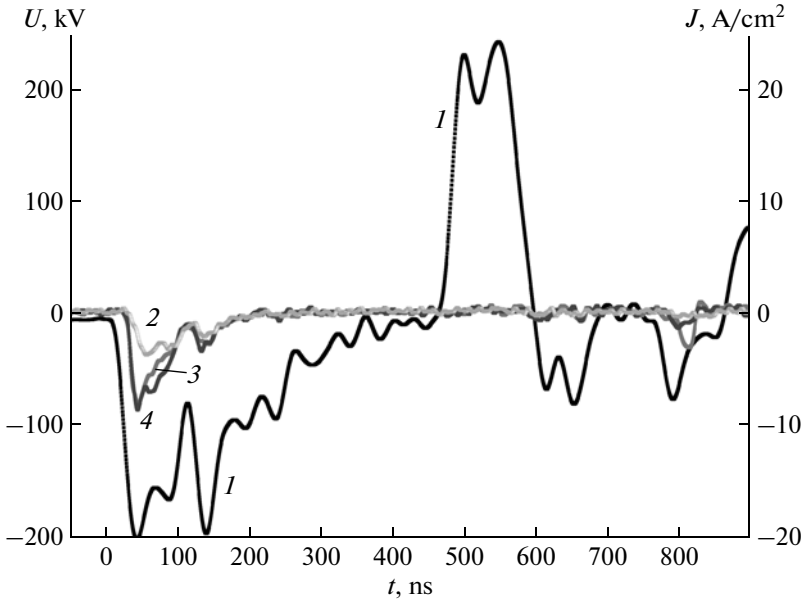

Fig. 6. Waveforms of the (*1*) accelerating voltage and (*2*–*4*) density of the current recorded with three Faraday cups, which were closed with an Al foil.

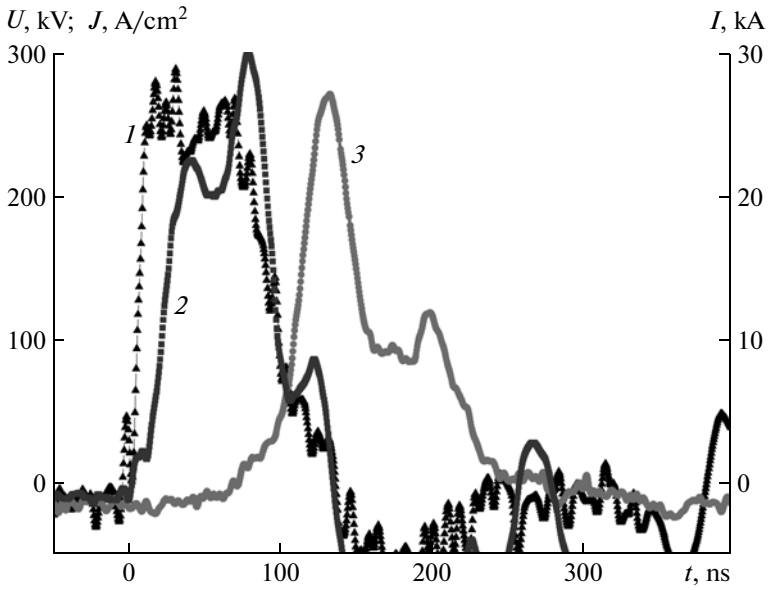

Fig. 7. Waveforms of the (*1*) accelerating voltage, (*2*) total current, and (*3*) ion-current density in the diode with external magnetic insulation.

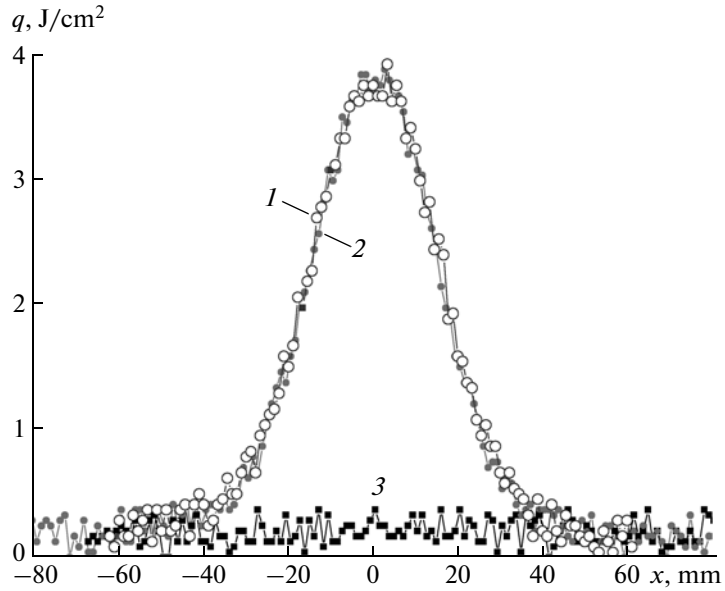

Fig. 8. The PIB energy-density distribution at the focus in the (*1*) horizontal and (*2*) vertical sections. Curve *3* is the initial thermal background of the target.

the contribution of the explosion-emission plasma to the target heating is insignificant.

PIB ENERGY DENSITY IN THE DIODE WITH EXTERNAL MAGNETIC INSULATION

The designed thermal-imaging procedure was used for studying the PIB, formed by an ion diode with external magnetic insulation [16]. The studies were performed on the ТЕМП-4М accelerator with the use of the same diagnostic equipment as for studies of an ion diode with the self-magnetic insulation. The waveforms that characterize operation of the ion diode with the self-magnetic insulation are given in Fig. 7.

The obtained data allow one to estimate the ion-beam energy density. The amplitude of the accelerating voltage during the PIB generation varies insignificantly (see Fig. 7); therefore, the pulse shape variation of the ion current density may not be taken into account during transportation. In this case, to calcu-

late the PIB energy density in the Origin 7.5 program, we shift the current-density waveform (curve *3* in Fig. 7) by the value equal to the average traveling time of accelerated ions from the diode to the CFC. Then, we calculate the integral of the product of the accelerating voltage by the ion-current density. For data of Fig. 7, the calculated energy density was 3.4 J/cm^2. Figure 8 demonstrates the measurement results of the PIB energy density by the thermal-imaging procedure.

The performed studies showed that for the diode with external magnetic insulation, the PIB energy density, calculated from the CFC readouts coincides (within the measurement accuracy) with the data obtained using the thermal-imaging procedure. The integration of the product of the ion-current density by the accelerating voltage during the PIB generation gives an energy density of 3.4 J/cm^2. According to the thermal-imaging measurements the energy density of the ion beam at the focus reaches 3.6–3.8 J/cm^2. Small disagreements can be attributed to an inaccurate PIB focusing in the entrance aperture of the CFC. The PIB density values, measured by two independent procedures, correspond to the data obtained in [4] for the diode of similar design.

CONCLUSION

The performed studies showed that the thermal-imaging diagnostics of parameters of the gigawatt-power pulse ion beams is an efficient prompt monitoring method. It is intended to measure the complete PIB energy and energy-density distribution on the target, optimize the operation of the ion diode, and control the target irradiation mode. The spatial resolution is 0.9–1.0 mm, the sensitivity of a typical infrared camera ensures recording of the thermal print for one pulse with an energy density higher than 0.02 J/cm^2. The contribution of electrons, generated during the second pulse, and explosion-emission plasma to the target heating does not exceed 0.05–0.08 J/cm^2 for operation of the diode in the single- and double-pulse modes. The thermal-imaging diagnostics does not require expensive consumed materials. The measurement time does not exceed 0.1 s; therefore, this diagnostics can be used for the prompt evaluation of the energy-density distribution of a powerful ion beam and during automation of the product processing with monitoring of irradiation parameters in each pulse.

ACKNOWLEDGMENTS

This work was supported by the Russian Foundation for Basic Research, project no. 12-08-31335.

REFERENCES

1. Bystritskii, V.M. and Didenko, A.N., *Moshchnye ionnye puchki* (High-power ion beams), Moscow: Energoatomizdat, 1984.
2. Christodoulides, C.E. and Freeman, J.H., *Nucl. Instrum. Methods Phys. Res.*, 1976, vol. 135, no. 1, p. 13.
3. Moskalev, V.A. and Sergeev, G.I., *Izmerenie parametrov puchkov zaryazhennykh chastits* (Measurement of charged particle beam parameters), Moscow: Energoatomizdat, 1991.
4. Davis, H.A., Bartsch, R.R., Olson, J.C., et al., *J. Appl. Phys.*, 1997, vol. 82, no. 7, p. 3223.
5. Remnev, G.E., Isakov, I.F., and Pushkarev, A.I., et al., *Surf. Coat. Technol.,* 1999, vol. 114, p. 206.
6. Pushkarev, A.I., Tarbokov, V.A., and Sazonov, R.V., RF Patent 86374, *Byull. Izobret.*, 2009, no. 24.
7. Isakova, Yu.I., Pushkarev, A.I., and Tarbokov, V.A., *Izv. Tomsk. Politekhn. Univ.*, 2010, vol. 316, no. 2, p. 76.
8. Isakova, Yu.I., Pushkarev, A.I., and Kholodnaya, G.E., *Instrum. Exper. Techn.*, 2011, vol. 54, no. 2, p. 183.
9. Pushkarev, A.I., Isakova, Yu.I., and Guselnikov, V.I., *Phys. Plasmas*, 2011, vol. 18, p. 083109.
10. Isakova, Y.I., *J. Korean Phys. Soc.,* 2011, vol. 59, no. 6, p. 3531.
11. Filippov, L.P., *Izmerenie teplofizicheskikh svoistv veshchestv metodom periodicheskogo nagreva* (Measurement of Thermal Properties of Matter by the Periodical Heating Method), Moscow: Energoatomizdat, 1984.
12. Proskurovskii, D.I., *Emissionnaya elektronika: Ucheb. posobie dlya vuzov* (Emission Electronics: A Manual. 2nd Ed.), Tomsk: Tomsk. Gos. Univ., 2010.
13. Pushkarev, A.I. and Sazonov, R.V., *Techn. Phys. Lett.,* 2007, vol. 34, no. 7, p. 44.
14. Belomyttsev, S.Ya., Korovin, S.D., and Mesyats, G.A., *Pis'ma Zh. Tekh. Fiz.,* 1980, vol. 6, no. 18, p. 1089.
15. Pushkarev, A.I., Novoselov, Yu.N., and Sazonov, R.V., *Instrum. Exper. Techn.*, 2007, vol. 50, no. 5, p. 687.
16. Lopatin, V.S., Remnev, G.E., Furman, E.G., et al., *Instrum. Exper. Techn.*, 2004, vol. 47, no. 4, p. 484.